

# Isomers in $^{203}\text{Tl}$ and core excitations built on a five-nucleon-hole structure

V. Bothe,<sup>1</sup> S.K. Tandel,<sup>1,2,\*</sup> S.G. Wahid,<sup>1</sup> P.C. Srivastava,<sup>3</sup> Bharti Bhoj,<sup>3</sup> P. Chowdhury,<sup>2</sup> R.V.F. Janssens,<sup>4,5</sup> F.G. Kondev,<sup>6</sup> M.P. Carpenter,<sup>6</sup> T. Lauritsen,<sup>6</sup> D. Seweryniak,<sup>6</sup> and S. Zhu<sup>6</sup>

<sup>1</sup>*School of Physical Sciences, UM-DAE Centre for Excellence in Basic Sciences, Mumbai 400098, India*

<sup>2</sup>*Department of Physics, University of Massachusetts Lowell, Lowell, Massachusetts 01854, USA*

<sup>3</sup>*Department of Physics, Indian Institute of Technology Roorkee, Roorkee 247667, India*

<sup>4</sup>*Department of Physics and Astronomy, University of North Carolina at Chapel Hill, Chapel Hill, North Carolina 27599, USA*

<sup>5</sup>*Triangle Universities Nuclear Laboratory, Duke University, Durham, North Carolina 27708, USA*

<sup>6</sup>*Argonne National Laboratory, Argonne, Illinois 60439, USA*

(Dated: November 27, 2024)

Isomers with three- and five-nucleon-hole configurations have been established in  $^{203}\text{Tl}$ . These include newly identified levels with a three-nucleon structure:  $I^\pi = (15/2^-)$  with  $T_{1/2} = 7.9(5)$  ns, and  $I^\pi = (35/2^-)$  with  $T_{1/2} = 4.0(5)$  ns. In addition, five-quasiparticle states:  $I^\pi = (39/2^-)$  with  $T_{1/2} = 1.9(2)$  ns, and  $I^\pi = (49/2^+)$  with  $T_{1/2} = 3.4(4)$  ns have also been established. The previously determined long-lived decay [ $T_{1/2} = 6.6(3)$   $\mu\text{s}$  from this work] is associated with isomerism of the  $I^\pi = (29/2^+)$  state. Levels above this long-lived isomer have been identified through a delayed-prompt coincidence measurement. Five-nucleon-hole states with excitation energies  $E_x \approx 7$  MeV have been established as well as possible octupole excitations of the  $^{208}\text{Pb}$  core built on these levels. The level scheme of  $^{203}\text{Tl}$  is extended up to  $E_x \approx 11$  MeV with the inclusion of 25 new transitions. Empirical and shell-model calculations have been performed to aid in the description of the observed states which are found to be predominantly of intrinsic character.

PACS numbers: 21.10.Re, 21.60.Ev, 23.20.Lv, 27.80.+w

## I. INTRODUCTION

The occurrence of metastable states in nuclei with proton or neutron numbers in the vicinity of shell closures is well established as arising from the presence of adjacent excited levels with a relatively large difference in angular momentum and small difference in energy. Isotopes of Hg ( $Z = 80$ ) and Tl ( $Z = 81$ ) with  $A \approx 200$ , lying just below the doubly-magic  $^{208}\text{Pb}$  nucleus in the periodic chart, are therefore good candidates for the observation of metastable states or isomers [1–5]. The proton-rich isotopes of Tl ( $A < 200$ ) are characterized by moderate oblate deformation on account of a significant number of valence neutrons leading to a small degree of collectivity [6, 7]. However, when approaching the  $N = 126$  shell gap, collective behavior is no longer evident. This is the case for isotopes of Tl near the line of stability, where  $^{203}\text{Tl}$  and  $^{205}\text{Tl}$  are the two stable isotopes [1–3, 8, 9]. The nucleus  $^{203}\text{Tl}$ , with  $N = 122$ , is only one proton and four neutron holes away from doubly-magic  $^{208}\text{Pb}$  and, as a result, its structure is expected to be dominated by single-particle excitations. The available valence orbitals are the proton  $s_{1/2}$ ,  $d_{3/2}$ ,  $d_{5/2}$  and  $h_{11/2}$  states and the neutron  $p_{1/2}$ ,  $p_{3/2}$ ,  $f_{5/2}$  and  $i_{13/2}$  ones. The presence of the unique-parity  $\pi h_{11/2}$  and  $\nu i_{13/2}$  orbitals allows for the realization of yrast, high-spin states, some of which may be of isomeric character, owing to hindrance induced by the angular momentum selection rule or a change in configuration.

The systematic delineation of isomers along an isotopic chain, most of which have relatively pure intrinsic character, provides a host of nuclear structure information, among which figure residual interactions between nucleons occupying different subshells. Heavy-ion and  $\alpha$ -induced reactions have been used to populate excited states at high spin in proton-rich Tl isotopes [7, 10]. However, in order to study isotopes near the line of stability, different reaction mechanisms such as inelastic excitation and multi-nucleon transfer may be utilized. In order to populate states with high spin, heavy projectiles with above-barrier energies are required. The isotopes of Tl approaching the shell closure at  $N = 126$ , particularly  $^{204,205}\text{Tl}$  [2, 3], have been studied up to high spin and several metastable states established. In contrast, there was limited knowledge on isomers in  $^{200-203}\text{Tl}$  prior to investigations by this collaboration. Recently, the observation of isomers with half-lives ranging from a few nanoseconds to hundreds of microseconds in  $^{200}\text{Tl}$  [11] and  $^{202}\text{Tl}$  [8] were reported. The existing information on  $^{203}\text{Tl}$  prior to the present work is limited, with levels up to possible spin  $(17/2) \hbar$  and excitation energy  $\approx 3$  MeV established through a deuteron-induced reaction [9], while a microsecond isomer was identified using projectile fragmentation [12]. In the former instance, the presence of a nanosecond isomer has been inferred, but its location was not established. In the latter case, no level scheme is reported, and a tentative assignment of  $I^\pi = (25/2^+)$  and a three-nucleon-hole character for the microsecond isomer is proposed. The motivation for the present work was to obtain unambiguous information on the structural aspects mentioned above in order to advance the understanding of the structure of  $^{203}\text{Tl}$ . An

\* Electronic address: sujit.tandel@cbs.ac.in ; sktandel@gmail.com

additional goal was to extend the level scheme of  $^{203}\text{Tl}$  to also encompass levels arising from the maximum possible number of nucleon-hole excitations, which is five in this case, which allows for discriminating tests of interactions used in shell-model calculations. Furthermore, it was also proposed to investigate the presence of possible octupole core excitations in  $^{203}\text{Tl}$  which would be built on five-nucleon-hole configurations. In this region, such excitations have thus far been observed only in  $^{203}\text{Hg}$  [4].

## II. EXPERIMENT AND DATA ANALYSIS

Multi-nucleon transfer reactions were used to populate excited states in  $^{203}\text{Tl}$ , with a 1450-MeV  $^{209}\text{Bi}$  beam from the ATLAS accelerator at Argonne National Laboratory, incident on a thick, 50 mg/cm<sup>2</sup> Au target. Gamma-ray coincidence data were recorded with the Gammasphere array comprising of 100 Compton-suppressed high-purity germanium detectors [13, 14]. In addition to prompt coincidence events, delayed data from the decay of isomeric levels were also recorded. In the first instance, the  $^{209}\text{Bi}$  beam, with the natural 82.5 ns pulsing from the ATLAS superconducting linear accelerator, was incident on the target for  $\approx 1$  ns, and then swept away for a 825-ns off period. Three- and higher-fold coincidence events were recorded within a 1  $\mu\text{s}$  coincidence window, allowing for the measurement of half-lives ranging from a few to several hundred nanoseconds. Later, two- and higher-fold coincidence data were collected only during beam-off periods by sweeping the beam with an ON/OFF ratio of 200  $\mu\text{s}$ /800  $\mu\text{s}$  via a free-running external clock, enabling the study of isomers with long ( $\mu\text{s}$ ) half-lives.

The coincidence data were sorted into a variety of histograms in order to establish the level structure and determine the half-lives of isomers using the TSCAN [15] and Radware [16] suite of programs. Three-dimensional histograms of prompt and delayed coincidence events were created and analyzed, corresponding to detection of all three  $\gamma$  rays within  $\pm 40$  ns and 50-650 ns of the trigger, respectively. To identify  $\gamma$  rays feeding the  $\mu\text{s}$  isomer, a three-dimensional histogram requiring two delayed transitions together with a prompt one, was constructed. The centroid-shift method was used to determine half-lives ranging between  $\approx 1$ -10 ns using an energy-gated two-dimensional histogram with energy on one axis and time difference of the associated transitions on the other. The coincidence relationships between  $\gamma$  rays deexciting the  $\mu\text{s}$  isomer were also analyzed with the help of a three-dimensional energy histogram consisting of transitions detected in the 800  $\mu\text{s}$  beam-off period. To determine the half-life of the  $\mu\text{s}$  isomer, several three-dimensional histograms spanning suitable time intervals within the 800  $\mu\text{s}$  beam-off period were created. Further details of data analysis methods are described elsewhere [17–19].

## III. RESULTS

Excited states in  $^{203}\text{Tl}$  up to medium spin and excitation energy of  $E_x \approx 3$  MeV had been identified earlier through the  $^{204}\text{Hg}(d,3n)$  reaction with an incident deuteron energy of  $\approx 25$  MeV [9], and projectile fragmentation using a 1 GeV/nucleon  $^{238}\text{U}$  beam on a thick  $^9\text{Be}$  target [12]. In the former, a cascade of  $\gamma$  rays with transition energies of 588, 533, 328, 350 and 265 keV were placed, in that order, above the  $11/2^-$  level at 1450 keV. The presence of an isomer with  $T_{1/2} = 7.9_{-13}^{+10}$  ns had been inferred, however its precise location had not been determined. From the projectile fragmentation work, feeding from a long-lived,  $T_{1/2} = 7.7(5)$   $\mu\text{s}$  isomer was reported and a spin-parity,  $I^\pi = (25/2^+)$ , was suggested. Though the above  $\gamma$  rays were observed, a level scheme was not reported.

The level scheme for  $^{203}\text{Tl}$  deduced from the present work is shown in Fig. 1. The presence of the two previously reported isomers is confirmed, and a slightly improved value of half-life is deduced for the  $\mu\text{s}$  isomer. The placement of the previously reported  $\gamma$  rays and level energies above the 588-keV,  $13/2^- \rightarrow 11/2^-$  transition, have been revised as described below, based on observed  $\gamma$  rays and their coincidence relationships in the three-dimensional energy histogram. A new level with  $E_x = 2048$  keV and possible spin-parity  $I^\pi = (15/2^-)$  is established. Several decay branches are observed from this state, including the 598-, 486- and 477-keV  $\gamma$  rays, along with an unobserved 10-keV transition to the  $I^\pi = 13/2^-$  level. From previous work [9, 12], the 350- and 265-keV  $\gamma$  rays were inferred to be in cascade above the 328- and 533-keV transitions. The present data unambiguously indicate that these 350- and 265-keV  $\gamma$  rays are not in mutual coincidence although they are coincident with all lower- and higher-lying transitions (Fig. 2). The presence of an unobserved 85-keV transition in cascade with the 265-keV line, but not with the 350-keV transition, was ascertained. One key evidence leading to the revised placements was the observation of a weak 798-keV  $\gamma$  ray which is found to be coincident with the 328-keV and all lower-lying transitions, but not with the 533-, 350- and 265-keV ones (Fig. 3). Another crucial indicator is the observation of a weak 334-keV transition in coincidence with all  $\gamma$  rays except with the 328-keV one (Fig. 4). The 334-keV transition is clearly visible in the delayed spectra but not in the prompt ones. These coincidence relationships, along with intensity balance arguments from the delayed data, justify the revision in the relative placement of the transitions. Further, inspection of the prompt spectra reveals that the intensity of the transitions reduces approaching closer to the  $(29/2^+)$  isomer, in the order 588, 350, 533, and 328 keV, respectively. The 334- and 798-keV  $\gamma$  rays may not have been identified in the previous work on account of their low intensity and proximity of the 798-keV  $\gamma$  ray to the strong,  $7/2^+ \rightarrow 3/2^+$ , 795-keV transition. The newly determined levels above the  $E_x = 2048$ -keV state are, there-

fore, the ones with  $E_x = 2134, 2399, 2932, 3260$  and  $3266$  keV and  $I^\pi = (19/2^-), (19/2^-), (23/2^-), (25/2^+)$  and  $(29/2^+)$ , respectively (Fig. 1). The 328-keV  $\gamma$  ray deexciting the 3260-keV level is assigned  $E1$  character from intensity balance considerations, as determined in the delayed spectra, with the  $3/2^+ \rightarrow 1/2^+$ , 279-keV transition (using its measured conversion coefficient) and the  $5/2^+ \rightarrow 1/2^+$ , 681-keV  $\gamma$  ray. Similar considerations lead to the determination of  $E2$  and  $M1$  character for the 350- and 265-keV transitions, and rule out other multipolarities. As stated above, the presence of an unobserved, 85-keV transition linking the 2134- and 2048-keV levels is inferred. For the isomeric, 334-keV  $\gamma$  ray, a  $(29/2^+) \rightarrow (23/2^-)$ ,  $E3$  assignment is implied. The presence of an unobserved 6-keV,  $(29/2^+) \rightarrow (25/2^+)$ ,  $E2$  transition, also deexciting the isomer is inferred. The  $\gamma$  rays observed following the deexcitation of the  $I^\pi = (29/2^+)$  isomer are listed in Table I.

The  $I^\pi = (15/2^-)$  state at  $E_x = 2048$  keV is determined to be isomeric with  $T_{1/2} = 7.9(5)$  ns, in agreement with the previously reported value [9]. The histogram of time difference of  $\gamma$  rays below and above this state and a comparison with prompt transitions of similar energy can be found in Fig. 5. Additionally, the data indicate the possibility of isomerism of the 2134-keV level, with a half-life up to several nanoseconds, however the low intensity and energy of the transitions involved do not allow for precise estimation of the value. All  $\gamma$  rays below the  $(29/2^+)$  state are found to exhibit delayed feeding in the 800  $\mu$ s beam-off period. The integral variation in intensity with time of summed coincidence counts, with gates on the 232-, 265-, 279-, 328-, 533-, 588- and 795-keV  $\gamma$  rays is illustrated in Fig. 6. A value of  $T_{1/2} = 6.6(3)$   $\mu$ s is obtained, with an uncertainty that is slightly below the quoted one in the previous work, i.e. 7.7(5)  $\mu$ s [12]. The measured value is associated with the half-life of the  $I^\pi = (29/2^+)$  state.

Typically, the presence of an intervening long-lived ( $\sim \mu$ s or greater) isomer prevents the identification of  $\gamma$  rays feeding such a level. In this case, with the 1  $\mu$ s Gammasphere coincidence window and the 6.6(3)  $\mu$ s half-life, only a small number of coincidence events comprising  $\gamma$  rays below and above the isomer were recorded. By summing coincidence spectra with gates on two strong delayed transitions below the isomer in a three-dimensional histogram, several prompt  $\gamma$  rays feeding the isomer could be identified [Fig. 7(a)]. The following  $\gamma$  rays were found to be in coincidence with the delayed transitions as well as with each other: 965, 211, 530, 288, 947, 438 and 313 keV. Their ordering is based on total intensities inferred from  $\gamma$ -ray intensities, and multipolarities which, for low-energy transitions, are determined from intensity balance considerations after gating on the higher-lying, 2306-keV line, combined with theoretical conversion coefficients [20]. Detailed information on these transitions is presented in Fig. 1 and Table II. Though some random contaminant transitions are also present in Fig. 7(a), their origin was accounted for in terms of the deexcita-

tion of low-lying states from the strong reaction channels observed in the data. The spin-parity assignments of the levels above the  $(29/2^+)$  state are based on systematics [21] as described later and should be considered tentative. Figure 7(b) is the prompt coincidence spectrum with gates on the 530- and 965-keV transitions. Additionally, four other significantly weaker  $\gamma$  rays, with energies 466, 756, 1089 and 2306 keV, were also visible in prompt coincidence, and are found to be enhanced in the summed prompt coincidence spectrum with gates on transitions between the  $(29/2^+)$  and  $(49/2^+)$  levels [Fig. 7(c)]. The 2306-keV  $\gamma$  ray is found to be coincident with all the above prompt transitions and is placed above the  $(49/2^+)$  level based on intensity considerations. It is worth noting that similar transitions with energies 2207 and 2256 keV are observed above the four- and three-nucleon-hole states in  $^{204}\text{Tl}$  and  $^{205}\text{Tl}$ , respectively [2, 3].

The presence of three isomers above the  $I^\pi = (29/2^+)$  state (Fig. 1) with half-lives in the range of a few nanoseconds is deduced from an inspection of time differences of  $\gamma$  rays between the  $(29/2^+)$  and  $(49/2^+)$  levels (Fig. 8), and the following values have been obtained:

1.  $E_x = 4442$  keV,  $I^\pi = (35/2^-)$ ,  $T_{1/2} = 4.0(5)$  ns
2.  $E_x = 4972$  keV,  $I^\pi = (39/2^-)$ ,  $T_{1/2} = 1.9(2)$  ns
3.  $E_x = 6957$  keV,  $I^\pi = (49/2^+)$ ,  $T_{1/2} = 3.4(4)$  ns

It may be noted that the  $I^\pi = (29/2^+)$  state in  $^{203}\text{Tl}$  is the analog of the isomeric  $9^-$  levels in Pb isotopes [21–23].

## IV. DISCUSSION

### A. Isomeric states and configurations

The high-spin isomers in Tl isotopes can be understood as resulting from the coupling of the  $h_{11/2}$  proton hole to specific neutron configurations in the corresponding Pb isotones with, in particular, a major contribution from neutrons occupying the  $i_{13/2}$  subshell. The low-lying two-neutron-hole configurations in even- $A$  Pb isotopes are the  $\nu(i_{13/2}^{-1}, p_{1/2}^{-1})$ ,  $\nu(i_{13/2}^{-1}, f_{5/2}^{-1})$  and  $\nu i_{13/2}^{-2}$  ones leading to the realization of isomeric  $I^\pi = 7^-, 9^-$  and  $12^+$  states [21, 22]. The corresponding states in odd- $A$  Tl isotones have the configurations  $\pi h_{11/2}^{-1} \otimes \nu^2(7^-)$ ,  $\pi h_{11/2}^{-1} \otimes \nu^2(9^-)$ , and  $\pi h_{11/2}^{-1} \otimes \nu^2(12^+)$  leading to  $I^\pi = 25/2^+, 29/2^+$  and  $35/2^-$  levels. The  $25/2^+$  and  $35/2^-$  states in  $^{205}\text{Tl}$  have been determined to be isomeric with  $T_{1/2} = 2.6$   $\mu$ s and  $T_{1/2} = 235$  ns, respectively [2]. Since the  $29/2^+ \rightarrow 25/2^+$   $E2$  transition in  $^{205}\text{Tl}$  has an energy of 328 keV, the decay of the  $29/2^+$  level has been found to be prompt [2]. Analogous isomeric levels have not been identified in lighter, odd- $A$  Tl isotopes with mass  $A \leq 199$ , most likely due to the underlying weak oblate deformation and resultant collective structures. In

$^{201}\text{Tl}$ , the presence of such isomeric states has not yet been established [24], however their existence cannot be ruled out. In  $^{203}\text{Tl}$ , under discussion here, the observed long-lived decay, with  $T_{1/2} = 6.6 \mu\text{s}$ , is assigned to the  $29/2^+$  level. The excitation energies of the  $25/2^+$  levels in  $^{203,205}\text{Tl}$  are quite similar (3260 and 3291 keV, respectively). This may be understood as follows: the  $\pi h_{11/2}$  and  $\nu p_{1/2}$  quasiparticle energies in the two isotopes are quite similar, however the  $\nu i_{13/2}$  one in  $^{203}\text{Tl}$  is lower by virtue of its relative proximity to the neutron Fermi level in comparison to  $^{205}\text{Tl}$ . This difference is compensated to a significant extent by the fact that the neutron pair-gap energy in  $^{205}\text{Tl}$  is lower than that in  $^{203}\text{Tl}$  [25], leading to the observed similarity of the excitation energies of the  $25/2^+$  levels in the two isotopes. The small separation (6 keV) between the  $25/2^+$  and  $29/2^+$  levels in  $^{203}\text{Tl}$  is mirrored in  $^{204}\text{Pb}$ , where the  $7^-$  and  $9^-$  levels are 79 keV apart [21]. An important difference is that the  $9^-$  state is lower in  $^{204}\text{Pb}$  in contrast to the  $25/2^+$  level in  $^{203}\text{Tl}$ . The identification of the closely-spaced pair of levels with  $I^\pi = 25/2^+$  and  $29/2^+$  in  $^{203}\text{Tl}$  thus provides insight into the difference of the magnitude of residual interactions of the  $h_{11/2}$  proton with the respective two-neutron-hole configurations in  $^{204}\text{Pb}$ . The transition rates for the  $I^\pi = 29/2^+$  isomeric decays are consistent with Weisskopf estimates and those in neighboring nuclei, *e.g.*,  $B(E3)[334 \text{ keV}] = 5.8 \text{ W.u.}$  The unhindered  $E3$  decay likely implies a configuration change from  $\pi h_{11/2}^{-1} \otimes \nu^2(9^-)$  to  $\pi d_{5/2}^{-1} \otimes \nu^2(9^-)$  for the  $29/2^+ \rightarrow 23/2^-$  transition in  $^{203}\text{Tl}$ .

In  $^{203}\text{Tl}$ , there are four neutron holes in contrast to only two in  $^{205}\text{Tl}$ . Consequently, levels with one-proton and four-neutron-hole configurations are possible in  $^{203}\text{Tl}$ , unlike in  $^{205}\text{Tl}$  where only two neutron holes are present. As a result, in  $^{205}\text{Tl}$ , there is no intervening level between the  $29/2^+$  and  $35/2^-$  states, and the  $35/2^-$  state decays by a 1217-keV,  $E3$  transition, and is characterized by a half-life of  $T_{1/2} = 235(10) \text{ ns}$  [2]. The  $I^\pi = 35/2^-$  state represents the maximum spin achievable from a three-nucleon-hole configuration, resulting from one  $h_{11/2}$  proton and two  $i_{13/2}$  neutrons. This state is found to be isomeric in  $^{203}\text{Tl}$  as well, with  $T_{1/2} = 4.0(5) \text{ ns}$ . It decays to the  $33/2^+$  level which has a five-nucleon-hole configuration, with likely mixed character comprising  $\pi h_{11/2}^{-1} \otimes \nu(i_{13/2}^{-1}, f_{5/2}^{-2}, p_{1/2}^{-1})$  and  $\pi h_{11/2}^{-1} \otimes \nu(i_{13/2}^{-1}, f_{5/2}^{-1}, p_{3/2}^{-1}, p_{1/2}^{-1})$  configurations. All the levels above the  $35/2^-$  state must have configurations involving five or more nucleons. The observed isomerism of the  $39/2^-$  state may be qualitatively understood in terms of the hindrance induced by the change of two neutrons in the configurations of the initial and final states in each of these cases. The  $I^\pi = 49/2^+$  state most likely results from the coupling of  $\pi h_{11/2}^{-1} \otimes \nu^2(19^-)$ , with the neutron configuration corresponding to the relevant level established in the  $^{204}\text{Pb}$  isotone [21]. It is noteworthy that the level structure of  $^{203}\text{Tl}$  above the  $29/2^+$  state inferred from the present work is quite similar to the one associated with the strongest cascade above the analogous  $9^-$

level in  $^{204}\text{Pb}$  (Fig. 9).

## B. “Empirical” calculations

“Empirical” calculations, based on near-neighbor systematics, have been performed to estimate the energies of isomeric states. For this purpose, the average of 1-quasineutron energies from neighboring, odd- $A$  Pb isotopes ( $^{203,205}\text{Pb}$ ), and 1-quasiproton energies derived from the corresponding excited levels in  $^{203}\text{Tl}$ , were used [26–28]. The neutron pair-gap energies were obtained using the five-point formula involving odd-even mass differences [25]. To calculate the energies of states with multi-nucleon configurations, the relevant 1-quasiparticle energies were summed with the pair-gap energy, and appropriate corrections were incorporated for the residual interactions. The magnitude of residual interactions was determined from isomeric configurations in neighboring Tl and Pb isotopes and the following values were obtained:  $15/2^-$  (119 keV):  $\pi h_{11/2}^{-1} \otimes \nu(f_{5/2}^{-1}, p_{1/2}^{-1})$ ;  $25/2^+$  (204 keV):  $\pi h_{11/2}^{-1} \otimes \nu(i_{13/2}^{-1}, p_{1/2}^{-1})$ ;  $29/2^+$  (160 keV):  $\pi h_{11/2}^{-1} \otimes \nu(i_{13/2}^{-1}, f_{5/2}^{-1})$ ;  $35/2^-$  (13 keV):  $\pi h_{11/2}^{-1} \otimes \nu i_{13/2}^{-2}$ . The calculated energies of the above mentioned states and a comparison with experimental values is displayed in Fig. 10. Sufficient experimental data are not available to determine the residual interactions for the five-nucleon configuration responsible for the  $49/2^+$  [ $\pi h_{11/2}^{-1} \otimes \nu(i_{13/2}^{-3}, f_{5/2}^{-1})$ ] state. Therefore, the energy for this state has been obtained by summing the experimental value of the  $29/2^+$  state in  $^{203}\text{Tl}$  with that of the  $\nu i_{13/2}^{-2}$ ,  $12^+$  level in  $^{204}\text{Pb}$  [21]. While the empirical calculations underestimate the experimental energies in most cases, there is fair agreement between the two, with the deviations being less than 300 keV for all states.

## C. Shell-model calculations

Shell-model calculations have been performed for  $^{203}\text{Tl}$  employing the KHH7B [29] effective interaction. Since proton excitations across the  $Z = 82$  shell gap and neutron ones across the  $N = 126$  one were not allowed, the active orbitals in the shell-model calculations are  $d_{5/2}$ ,  $h_{11/2}$ ,  $d_{3/2}$  and  $s_{1/2}$  for protons, and  $i_{13/2}$ ,  $p_{3/2}$ ,  $f_{5/2}$ , and  $p_{1/2}$  for neutrons. The shell-model code Oxbash [30] was used for the diagonalization of the matrices of interest. The deviations of the predicted energies from the experimental values range between a few hundred keV to 0.5 MeV. The  $29/2^+$  state is calculated to be lower in energy than the  $25/2^+$  level, unlike what is displayed by the data (Fig. 10). A comparison of the excitation energies from experiment and those from both empirical and shell-model calculations is presented in Table III, along with the primary underlying configurations. The significant disagreement between the experimental and

calculated values for the  $29/2^+$  and  $35/2^-$  states indicates the need for improving the interactions used in the shell-model calculations.

#### D. Octupole core excitations

The level with  $E_x = 9263$  keV is assigned  $I^\pi = (55/2^-)$  and interpreted as the octupole excitation of the  $^{208}\text{Pb}$  core built on the  $\pi h_{11/2}^{-1} \otimes \nu(i_{13/2}^{-3}, f_{5/2}^{-1})$ ,  $I^\pi = 49/2^+$  configuration. The energy of the  $55/2^- \rightarrow 49/2^+$  transition (2306 keV) is consistent with this interpretation, as described below. Following the prescription outlined previously [2, 3, 31], the expected transition energy for the  $E3$  excitation built on the five-nucleon hole,  $49/2^+$  state can be estimated. While the unperturbed energy of the  $E3$  excitation in  $^{208}\text{Pb}$  would be 2615 keV, energy shifts would result from the coupling to configurations involving multiple nucleons. These can be expressed as the sum of energy shifts corresponding to the individual constituents of such a configuration. For instance, as described previously [3, 31], energy shifts of  $\Delta E = -150$  keV and  $+40$  keV are obtained based on the following transitions:  $17/2^+ \rightarrow 11/2^-$  (2465 keV) in  $^{207}\text{Tl}$ , and  $11/2^+ \rightarrow 5/2^-$  (2655 keV) in  $^{207}\text{Pb}$ , respectively. These transitions represent the stretched  $E3$  excitations built on the  $\pi h_{11/2}^{-1}$  and  $\nu f_{5/2}^{-1}$  states in  $^{207}\text{Tl}$  and  $^{207}\text{Pb}$ , respectively. For the  $\nu i_{13/2}^{-3}$  configuration, an energy shift of -262 keV has been estimated [3] since the  $E3$  excitation built on the  $\nu i_{13/2}^{-3}$ ,  $I^\pi = 33/2^+$  state has not been identified yet. Thus, for the  $\pi h_{11/2}^{-1} \otimes \nu(i_{13/2}^{-3}, f_{5/2}^{-1})$  configuration, an addition of the above mentioned energy shifts yields a value of -372 keV, implying an estimated  $55/2^- \rightarrow 49/2^+$ , 2243-keV transition energy. This estimated value is lower than the observed one by only 63 keV. The situation is similar to that observed for the  $\pi h_{11/2}^{-1} \otimes \nu(i_{13/2}^{-2}, f_{5/2}^{-1})$ ,  $I^\pi = 20^+$  configuration in  $^{204}\text{Tl}$  [3] where the estimated value is 61 keV lower than the experimental one. It is worth noting that even better agreement (within several keV) between estimated and experimental values is seen for the  $22^+$  state in  $^{204}\text{Tl}$  [3] and  $35/2^-$  level in  $^{205}\text{Tl}$  [2], *e.g.*, excitations involving high- $j$  orbitals only. This likely suggests an underestimation of the magnitude of the repulsive interaction of the stretched- $E3$  excitation with the  $f_{5/2}$  neutron hole. On the other hand, the reasonable agreement between estimated and experimental values appears to validate the assignment of the 2306-keV transition in  $^{203}\text{Tl}$  as the octupole core excitation

built on the  $45/2^+$  state.

## V. SUMMARY

The excited level structure of  $^{203}\text{Tl}$  has been considerably expanded and is now established up to high spin with the inclusion of 25 new transitions, five isomeric states, and octupole core excitations built on a five-nucleon-hole configuration. Isomeric states with  $I^\pi = (15/2^-)$ ,  $(35/2^-)$ ,  $(39/2^-)$  and  $(49/2^+)$ , and respective half-lives of  $T_{1/2} = 7.9(5)$  ns, 4.0(5) ns, 1.9(2) ns, and 3.4(4) ns, have been identified. The half-life of the previously determined long-lived decay is revised from 7.7(5) to 6.6(3)  $\mu\text{s}$ , and is associated with the  $I^\pi = (29/2^+)$  state. The structure of the levels fed by this long-lived decay is significantly modified. Gamma rays feeding the 6.6  $\mu\text{s}$  isomer have been identified through delayed-prompt coincidence measurements. Of particular note is the observation of octupole core excitations built on a five-nucleon hole configuration. ‘‘Empirical’’ calculations, based on near-neighbor systematics, are able to satisfactorily reproduce key states in the experimental level scheme, while those using the shell model appear to significantly underestimate the state energies in two instances. These results contribute valuable information towards improving the understanding of nuclear structure in the vicinity of the heaviest doubly-magic nucleus,  $^{208}\text{Pb}$ .

## VI. ACKNOWLEDGMENTS

The authors wish to thank I. Ahmad, J.P. Greene, T.L. Khoo, A.J. Knox, C.J. Lister, D. Peterson, U. Shirwadkar, X. Wang and C.M. Wilson for assistance during the experiment. V.B. acknowledges assistance under the INSPIRE fellowship of the Department of Science and Technology, Government of India. S.K.T. would like to acknowledge support from the University Grants Commission, India, under the Faculty Recharge Programme. S.G.W. acknowledges support from the DST-INSPIRE Ph.D. Fellowship of the Department of Science and Technology, Government of India (Fellowship No. IF150098). This work is supported by the U.S. Department of Energy, Office of Science, Office of Nuclear Physics, under award numbers DE-FG02-94ER40848 and DE-FG02-94ER40834 (UML), DE-FG02-97ER41041 (UNC) and DE-FG02-97ER41033 (TUNL), and contract number DE-AC02-06CH11357 (ANL). The research described here utilized resources of the ATLAS facility at ANL, which is a DOE Office of Science user facility.

[1] O. Häusser, J.R. Beene, T.K. Alexander, A.B. McDonald, and T. Faestermann, Phys. Lett. B **64**(3), 273

(1976).

- [2] J. Wrzesiński, R. Broda, B. Fornal, W. Kròlas, T. Pawlat, M.P. Carpenter, R.V.F. Janssens, D. Seweryniak, S. Lunardi, C.A. Ur, *et al*, Eur. Phys. J. A **20**, 57 (2004).
- [3] R. Broda, K.H. Maier, B. Fornal, J. Wrzesiński, B. Szpak, M.P. Carpenter, R.V.F. Janssens, W. Kròlas, T. Pawlat, and S. Zhu, Phys. Rev. C **84**, 014330 (2011).
- [4] B. Szpak, K. H. Maier, A. S. Smolkowska, B. Fornal, R. Broda, M. P. Carpenter, N. Cieplicka, R. V. F. Janssens, W. Krolas, T. Pawlat, J. Wrzesiński, and S. Zhu, Phys. Rev. C **83**, 064315 (2011).
- [5] J. Wrzesiński, G.J. Lane, K.H. Maier, R.V.F. Janssens, G.D. Dracoulis, R. Broda, A.P. Byrne, M.P. Carpenter, R.M. Clark, M. Cromaz, *et al*, Phys. Rev. C **92**, 044327 (2015).
- [6] A.J. Kreiner, M. Fenzl, S. Lunardi, and M.A.J. Mariscotti, Nucl. Phys. A **282**, 243 (1977).
- [7] E.A. Lawrie, P.A. Vymers, Ch. Vieu, J.J. Lawrie, C. Schück, R.A. Bark, R. Lindsay, G.K. Mabala, S.M. Maliage, P.L. Masiteng, *et al*, Eur. Phys. J. A **45**, 39 (2010).
- [8] S.G. Wahid, S. K. Tandel, Saket Suman, M. Hemalatha, Anurag Patel, Poulomi Roy, A. Y. Deo, Pragati, P. C. Srivastava, Bharti Bhoy, S. S. Bhattacharjee, R. P. Singh, S. Muralithar, P. Chowdhury, R. V. F. Janssens, M. P. Carpenter, T. L. Khoo, F. G. Kondev, T. Lauritsen, C. J. Lister, D. Seweryniak, S. Zhu, S. Rai, A. Sharma, Phys. Rev. C **102**, 024329 (2020).
- [9] M.G. Slocombe, J.O. Newton, and G.D. Dracoulis, Nucl. Phys. A **275**, 166 (1977).
- [10] A.J. Kreiner, M.A.J. Mariscotti, C. Baktash, E. der Mateosian, and P. Thieberger, Phys. Rev. C **23**, 748 (1981).
- [11] Poulomi Roy, S.K. Tandel, Saket Suman, P. Chowdhury, R.V.F. Janssens, M.P. Carpenter, T.L. Khoo, F.G. Kondev, T. Lauritsen, C.J. Lister, *et al*, Phys. Rev. C **100**, 024320 (2019).
- [12] M. Pfutzner *et al.*, Phys. Lett. B **444**, 32 (1998).
- [13] I-Yang Lee, Nucl. Phys. A **520**, c641 (1990).
- [14] R.V.F. Janssens and F.S. Stephens, Nucl. Phys. News **6**, 9 (1996).
- [15] H.-Q. Jin, TSCAN and related programs, RUTGERS-ORNL-UTK, 1992-1997.
- [16] D. C. Radford, Nucl. Instr. and Meth. A **361**, 297 (1995).
- [17] S. K. Tandel *et al.*, Phys. Lett. B **750**, 225 (2015).
- [18] S. K. Tandel *et al.*, Phys. Rev. C **94**, 064304 (2016).
- [19] S. G. Wahid *et al.*, Phys. Rev. C **92**, 054323 (2015).
- [20] T. Kibedi, T.W. Burrows, M.B. Trzhaskovskaya, P.M. Davidson, C.W. Nestor, Jr., Nucl. Instr. and Meth. A **589**, 202 (2008).
- [21] C.G. Linden, I. Bergstrom, J. Blomqvist, and C. Roulet, Z. Phys. A **284**, 217 (1978).
- [22] R. Lutter, O. Hausser, D.J. Donahue, R.L. Hershberger, F. Riess, H. Bohn, T. Faestermann, F.V. Feilitzsch, K.E.G. Lobner, Nucl. Phys. A **229**, 230 (1974).
- [23] U. Rosengård, P. Carlè, A. Källberg, L.O. Norlin, K.G. Rensfelt, H.C. Jain, B. Fant, and T. Weckström, Nucl. Phys. A **482**, 573 (1988).
- [24] S. Das Gupta, S. Bhattacharyya, H. Pai, G. Mukherjee, Soumik Bhattacharya, R. Palit, A. Shrivastava, A. Chatterjee, S. Chanda, V. Nanal, *et al*, Phys. Rev. C **88**, 044328 (2013).
- [25] P. Moller and J.R. Nix, Nucl. Phys. A **536**, 20 (1992).
- [26] F.G. Kondev, Nuclear Data Sheets **108**, 365 (2007).
- [27] F.G. Kondev, Nuclear Data Sheets **105**, 1 (2005).
- [28] F.G. Kondev, Nuclear Data Sheets **166**, 1 (2020).
- [29] G. H. Herling and T. T. S. Kuo, Nucl. Phys. A **181**, 113 (1972).
- [30] B.A. Brown, Oxbash for Windows, MSU-NSCL Report 1289, 2004.
- [31] M. Kadi, P. E. Garrett, Minfang Yeh, S. W. Yates, T. Belgya, A. M. Oros-Peusquens, and K. Heyde, Phys. Rev. C **61**, 034307 (2000).

TABLE I: Energies and intensities of  $\gamma$  rays, and excitation energies and spins of initial and final states in  $^{203}\text{Tl}$  up to the  $6.6 \mu\text{s}$  isomer. Transition energies are accurate to within 0.5 keV. Statistical uncertainties on  $\gamma$ -ray intensities are listed. Relative intensities have been obtained from data in the delayed regime. Transition multipolarities determined from intensity balance considerations are noted.

| $E_\gamma$ (keV) | $E_i$ (keV) | $\rightarrow$ | $E_f$ (keV) | $I_i^\pi$            | $\rightarrow$ | $I_f^\pi$            | $I_\gamma$ | Multipolarity |
|------------------|-------------|---------------|-------------|----------------------|---------------|----------------------|------------|---------------|
| (6)              | 3266        | $\rightarrow$ | 3260        | (29/2 <sup>+</sup> ) | $\rightarrow$ | (25/2 <sup>+</sup> ) | –          |               |
| (10)             | 2048        | $\rightarrow$ | 2038        | (15/2 <sup>-</sup> ) | $\rightarrow$ | (13/2 <sup>-</sup> ) | –          |               |
| (33)             | 1218        | $\rightarrow$ | 1184        | 9/2 <sup>+</sup>     | $\rightarrow$ | 7/2 <sup>+</sup>     | –          |               |
| (85)             | 2462        | $\rightarrow$ | 2376        | (19/2 <sup>-</sup> ) | $\rightarrow$ | (15/2 <sup>-</sup> ) | –          |               |
| 114.9            | 2048        | $\rightarrow$ | 1933        | (15/2 <sup>-</sup> ) | $\rightarrow$ | –                    | –          |               |
| 143.5            | 1218        | $\rightarrow$ | 1074        | 9/2 <sup>+</sup>     | $\rightarrow$ | 7/2 <sup>+</sup>     | 11(3)      |               |
| 232.1            | 1450        | $\rightarrow$ | 1218        | 11/2 <sup>-</sup>    | $\rightarrow$ | 9/2 <sup>+</sup>     | 84(5)      |               |
| 265.0            | 2399        | $\rightarrow$ | 2134        | (19/2 <sup>-</sup> ) | $\rightarrow$ | (19/2 <sup>-</sup> ) | 27(3)      | <i>M1</i>     |
| 279.3            | 279         | $\rightarrow$ | 0           | 3/2 <sup>+</sup>     | $\rightarrow$ | 1/2 <sup>+</sup>     | 84(4)      |               |
| 327.9            | 3260        | $\rightarrow$ | 2932        | (25/2 <sup>+</sup> ) | $\rightarrow$ | (23/2 <sup>-</sup> ) | 100(5)     | <i>E1</i>     |
| 333.7            | 3266        | $\rightarrow$ | 2932        | (29/2 <sup>+</sup> ) | $\rightarrow$ | (23/2 <sup>-</sup> ) | 4(1)       |               |
| 350.2            | 2399        | $\rightarrow$ | 2048        | (19/2 <sup>-</sup> ) | $\rightarrow$ | (15/2 <sup>-</sup> ) | 54(4)      | <i>E2</i>     |
| 362.1            | 1933        | $\rightarrow$ | 1571        | –                    | $\rightarrow$ | –                    | –          |               |
| 378.3            | 1562        | $\rightarrow$ | 1184        | –                    | $\rightarrow$ | 7/2 <sup>+</sup>     | –          |               |
| 387.1            | 1571        | $\rightarrow$ | 1184        | –                    | $\rightarrow$ | 7/2 <sup>+</sup>     | 3(1)       |               |
| 401.4            | 681         | $\rightarrow$ | 279         | 5/2 <sup>+</sup>     | $\rightarrow$ | 3/2 <sup>+</sup>     | 10(2)      |               |
| 477.3            | 2048        | $\rightarrow$ | 1571        | (15/2 <sup>-</sup> ) | $\rightarrow$ | –                    | 7(2)       |               |
| 485.8            | 2048        | $\rightarrow$ | 1562        | (15/2 <sup>-</sup> ) | $\rightarrow$ | –                    | 4(1)       |               |
| 488.2            | 1562        | $\rightarrow$ | 1074        | –                    | $\rightarrow$ | 7/2 <sup>+</sup>     | –          |               |
| 496.8            | 1571        | $\rightarrow$ | 1047        | –                    | $\rightarrow$ | 7/2 <sup>+</sup>     | 7(2)       |               |
| 503.8            | 1184        | $\rightarrow$ | 681         | 7/2 <sup>+</sup>     | $\rightarrow$ | 5/2 <sup>+</sup>     | 6(1)       |               |
| 533.1            | 2932        | $\rightarrow$ | 2399        | (23/2 <sup>-</sup> ) | $\rightarrow$ | (19/2 <sup>-</sup> ) | 85(6)      | <i>E2</i>     |
| 537.3            | 1218        | $\rightarrow$ | 681         | 9/2 <sup>+</sup>     | $\rightarrow$ | 5/2 <sup>+</sup>     | 10(2)      |               |
| 588.5            | 2038        | $\rightarrow$ | 1450        | (13/2 <sup>-</sup> ) | $\rightarrow$ | 11/2 <sup>-</sup>    | 90(6)      |               |
| 598.5            | 2048        | $\rightarrow$ | 1450        | (15/2 <sup>-</sup> ) | $\rightarrow$ | 11/2 <sup>-</sup>    | 4(1)       |               |
| 680.6            | 681         | $\rightarrow$ | 0           | 5/2 <sup>+</sup>     | $\rightarrow$ | 1/2 <sup>+</sup>     | 5(1)       |               |

| $E_\gamma$ (keV) | $E_i$ (keV) | $\rightarrow$ | $E_f$ (keV) | $I_i^\pi$  | $\rightarrow$ | $I_f^\pi$  | $I_\gamma$ | Multipolarity |
|------------------|-------------|---------------|-------------|------------|---------------|------------|------------|---------------|
| 794.8            | 1074        | $\rightarrow$ | 279         | $7/2^+$    | $\rightarrow$ | $3/2^+$    | 65(5)      |               |
| 797.6            | 2932        | $\rightarrow$ | 2134        | $(23/2^-)$ | $\rightarrow$ | $(19/2^-)$ | 14(3)      |               |
| 905.2            | 1184        | $\rightarrow$ | 279         | $7/2^+$    | $\rightarrow$ | $3/2^+$    | 22(3)      |               |

TABLE II: Energies and intensities of  $\gamma$  rays, and excitation energies and spins of initial and final states in  $^{203}\text{Tl}$  above the 6.6  $\mu\text{s}$  isomer. Transition energies are accurate to within 0.5 keV. Statistical uncertainties on  $\gamma$ -ray intensities are listed. Relative intensities have been obtained primarily from data in the prompt regime. The intensities in Tables I and II should be read independently of each other.

| $E_\gamma$ (keV) | $E_i$ (keV) | $\rightarrow$ | $E_f$ (keV) | $I_i^\pi$  | $\rightarrow$ | $I_f^\pi$  | $I_\gamma$ |
|------------------|-------------|---------------|-------------|------------|---------------|------------|------------|
| 211.0            | 4442        | $\rightarrow$ | 4231        | $(35/2^-)$ | $\rightarrow$ | $(33/2^+)$ | 68(9)      |
| 287.7            | 5260        | $\rightarrow$ | 4972        | $(41/2^-)$ | $\rightarrow$ | $(39/2^-)$ | 32(2)      |
| 312.7            | 6957        | $\rightarrow$ | 6644        | $(49/2^+)$ | $\rightarrow$ | $(45/2^+)$ | 17(2)      |
| 437.6            | 6644        | $\rightarrow$ | 6207        | $(45/2^+)$ | $\rightarrow$ | $(43/2^-)$ | 26(2)      |
| 466.0            | 9729        | $\rightarrow$ | 9263        | –          | $\rightarrow$ | $(55/2^-)$ | –          |
| 530.3            | 4972        | $\rightarrow$ | 4442        | $(39/2^-)$ | $\rightarrow$ | $(35/2^-)$ | 66(4)      |
| 755.6            | 11107       | $\rightarrow$ | 10352       | –          | $\rightarrow$ | –          | –          |
| 947.2            | 6207        | $\rightarrow$ | 5260        | $(43/2^-)$ | $\rightarrow$ | $(41/2^-)$ | 31(3)      |
| 965.2            | 4231        | $\rightarrow$ | 3266        | $(33/2^+)$ | $\rightarrow$ | $(29/2^+)$ | 100(16)    |
| 1088.9           | 10352       | $\rightarrow$ | 9263        | –          | $\rightarrow$ | $(55/2^-)$ | –          |
| 2305.7           | 9263        | $\rightarrow$ | 6957        | $(55/2^-)$ | $\rightarrow$ | $(49/2^+)$ | 11(3)      |

TABLE III: Energies and spins of isomeric levels in  $^{203}\text{Tl}$  from experiment, “empirical” and shell-model calculations (see text for details).

| $I_i^\pi$ | $T_{1/2}$            | Configuration                                      | $E_{exp}$ (keV) | $E_{emp}$ (keV) | $E_{SM}$ (keV) |
|-----------|----------------------|--|-----------------|-----------------|----------------|
| $15/2^-$  | 7.9(5) ns            | $\pi s_{1/2}^{-1} \nu p_{1/2}^{-1} i_{13/2}^{-1}$  | 2048            | 2185            | 1827           |
| $29/2^+$  | 6.6(3) $\mu\text{s}$ | $\pi h_{11/2}^{-1} \nu f_{5/2}^{-1} i_{13/2}^{-1}$ | 3266            | 2999            | 2803           |
| $35/2^-$  | 4.0(5) ns            | $\pi h_{11/2}^{-1} \nu i_{13/2}^{-2}$              | 4442            | 4148            | 3899           |
| $49/2^+$  | 3.4(4) ns            | $\pi h_{11/2}^{-1} \nu f_{5/2}^{-1} i_{13/2}^{-3}$ | 6957            | 6782            | 6627           |



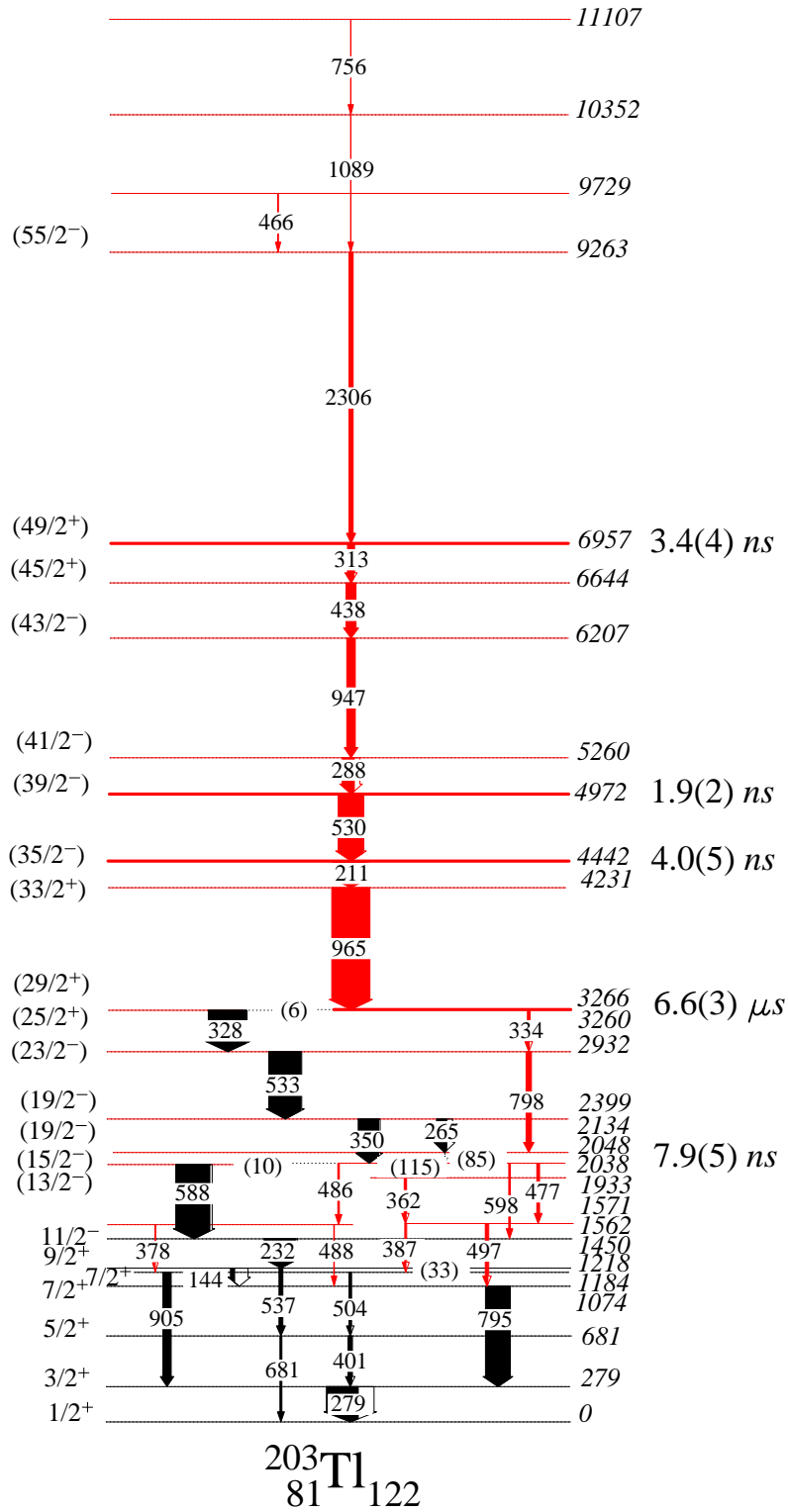


FIG. 1: Partial level scheme of  $^{203}\text{Tl}$  obtained from the present work. The transitions and levels above the  $(29/2^+)$  isomeric state, and several below it (marked in red), are newly established.

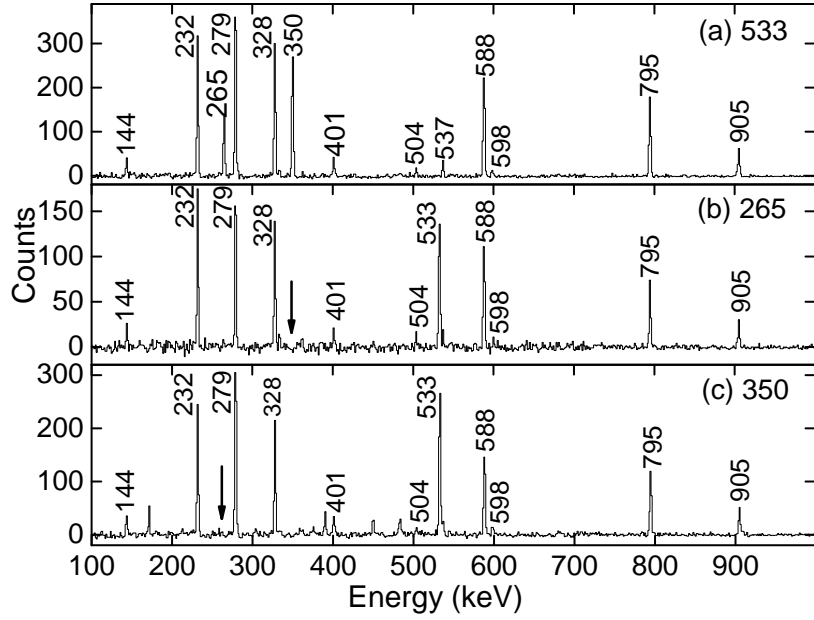


FIG. 2: Double-gated summed coincidence spectra showing  $\gamma$  rays in coincidence with the: (a) 533- (b) 265- (c) 350-keV transitions, together with any of the 232, 328 and 588-keV transitions. It is evident that the 265 and 350 keV transitions, the positions of which are marked with arrows in the middle and lower panels, are not coincident with each other as previously proposed [9, 12].

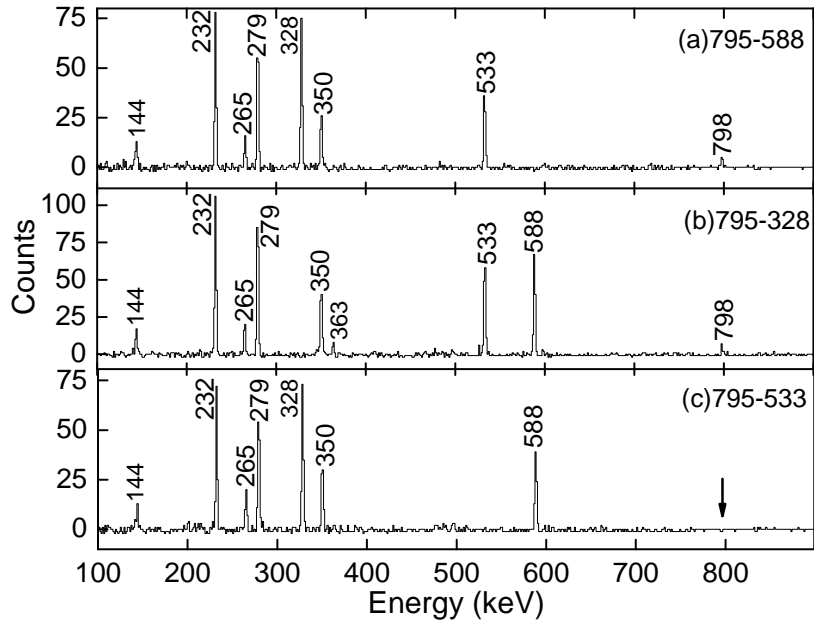


FIG. 3: Double-gated coincidence spectra, with gates on the transitions indicated in the panels, illustrating that the newly observed 798-keV  $\gamma$  ray is coincident with the 588- and 328-keV transitions, but not with the 533-keV one (arrow).

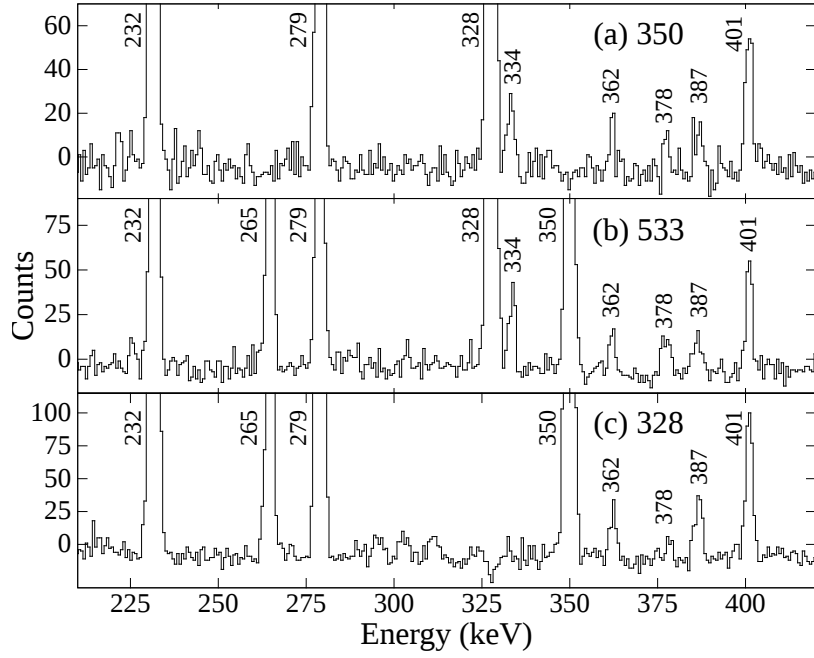


FIG. 4: Double-gated coincidence spectra, with gates on the  $\gamma$  rays indicated in the panels, highlighting the presence of the 334-keV isomeric transition in the 350- and 533-keV gated spectra, and its absence in the 328-keV gated spectrum.

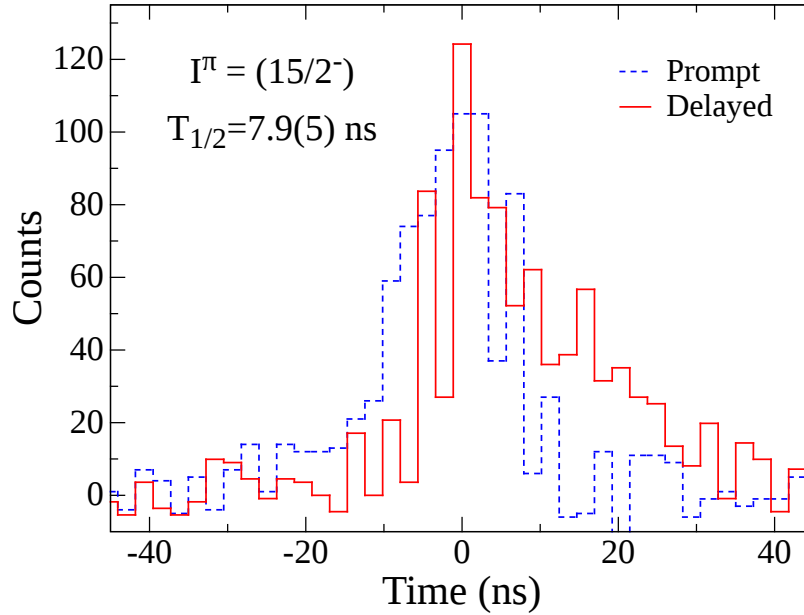


FIG. 5: Half-life of the  $I^\pi = (15/2^-)$  level measured using the centroid-shift method. The time difference between the 588- and 350-keV transitions, below and above this state, respectively, is displayed in red, while that of two prompt  $\gamma$  rays with similar energies is shown in blue. A value of  $T_{1/2} = 7.9(5)$  ns is inferred.

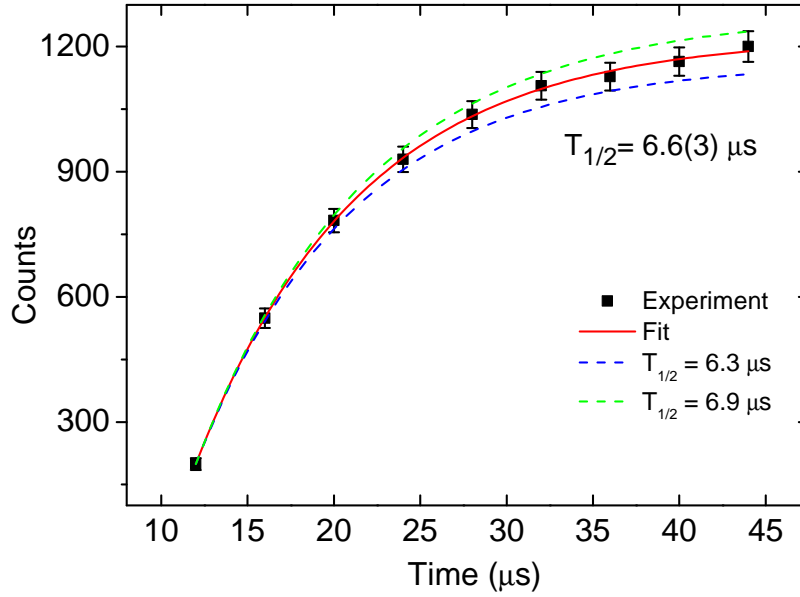


FIG. 6: Variation with time of the cumulative intensity of  $\gamma$  rays from the long-lived,  $\mu\text{s}$  decay. A half-life of  $6.6(3)$   $\mu\text{s}$  is deduced for the  $(29/2^+)$  state.

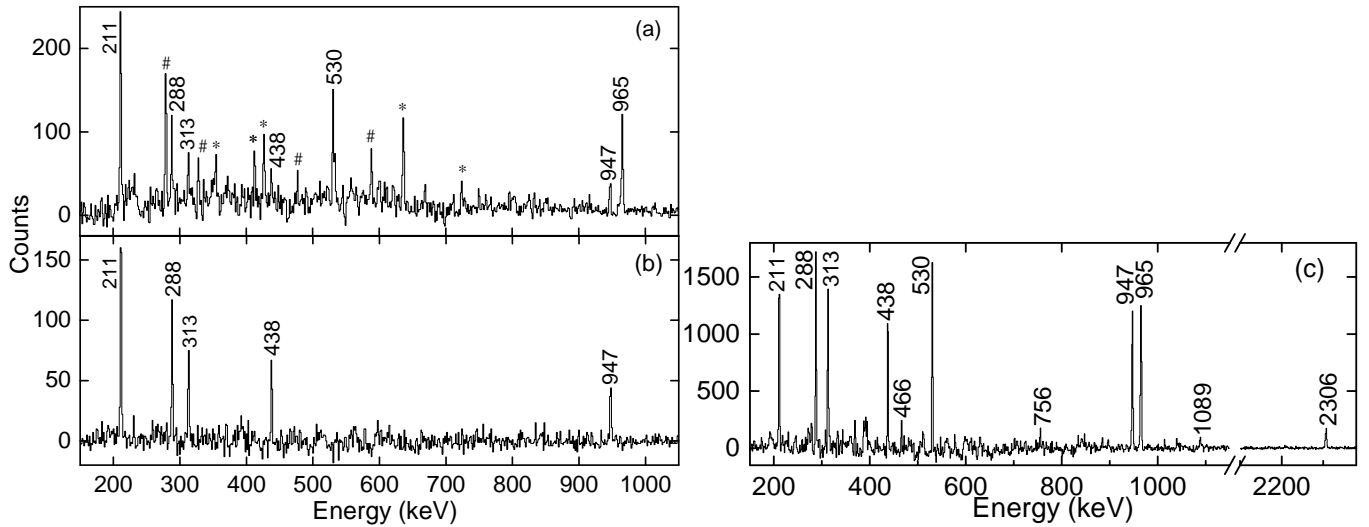


FIG. 7: (a) Summed delayed-prompt coincidence spectrum with gates on the 232-, 265-, 328-, 533-, 588- and 795-keV transitions in the delayed regime. Prompt  $\gamma$  rays, feeding the  $\mu\text{s}$  isomer, observed in coincidence with these delayed transitions, are displayed. The hash marks indicate strong transitions deexciting the isomer while the asterisks denote known contaminant  $\gamma$  rays from other reaction channels. (b) Prompt coincidence spectrum with a double gate on the 530- and 965-keV transitions. (c) Double-gated prompt coincidence spectrum obtained by summing gates on strong transitions above the  $\mu\text{s}$  isomer and below the  $(49/2^+)$  level.

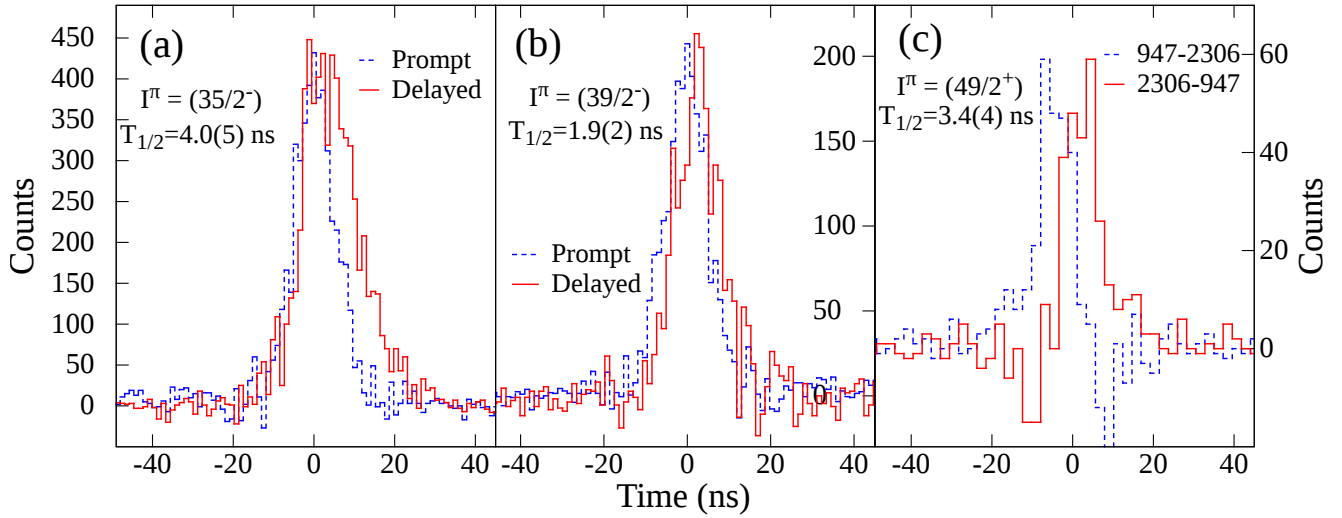


FIG. 8: Half-lives of the  $I^\pi = (35/2^-)$ ,  $(39/2^-)$  and  $(49/2^+)$  levels determined using the centroid-shift method. In panels (a) and (b), the histogram in red (solid line) indicates the time difference of  $\gamma$  rays below and above the relevant states while the one in blue (dashed line) corresponds to that of prompt transitions with similar energy. Values of  $T_{1/2} = 4.0(5)$  ns and  $1.9(2)$  ns are determined for the  $(35/2^-)$  and  $(39/2^-)$  levels based on the observed centroid shifts. In panel (c), the time difference between the 947- and 2306-keV  $\gamma$  rays and vice versa are compared which is equal to twice the mean life of the  $I^\pi = (49/2^+)$  level, leading to a value of  $T_{1/2} = 3.4(4)$  ns for this state.

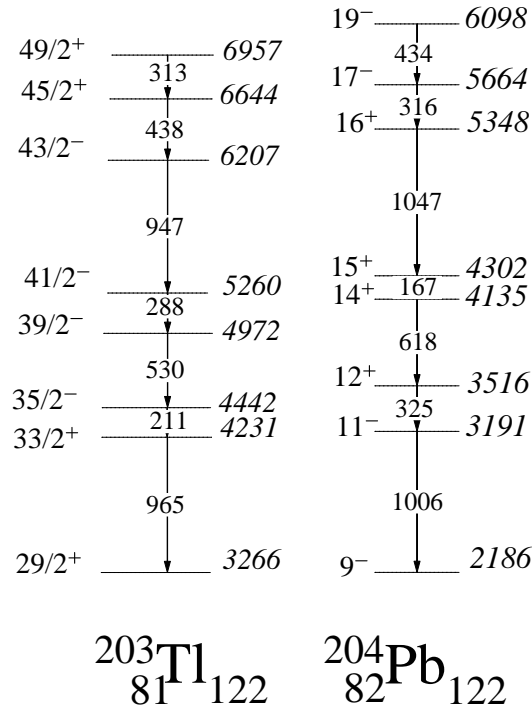


FIG. 9: Comparison of the level structure above the analogous  $29/2^+$  and  $9^-$  isomeric states in  $^{203}\text{Tl}$  and  $^{204}\text{Pb}$ , respectively.

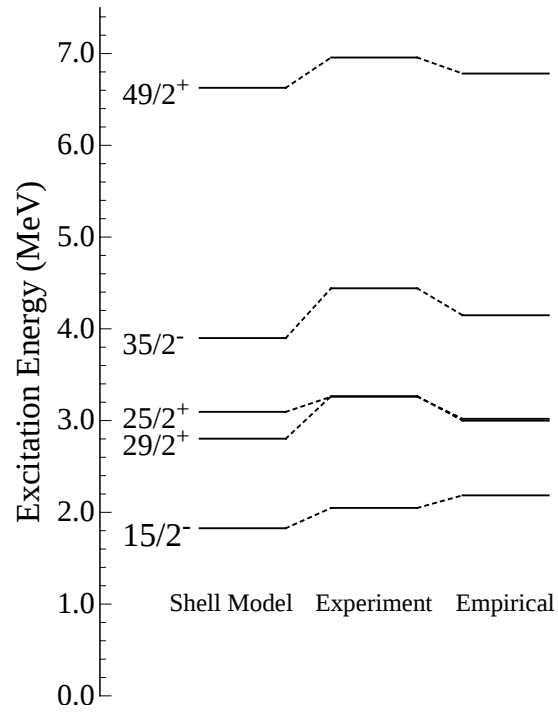


FIG. 10: Excitation energies of selected states in  $^{203}\text{Tl}$  obtained from experiment and their comparison with empirical and shell-model calculations discussed in the text.